Mycoplasma promotes malignant transformation in vivo, and its DnaK, a bacterial chaperone protein, has broad oncogenic properties

Davide Zella[a,b,1], Sabrina Curreli[a,c], Francesca Benedetti[a,b], Selvi Krishnan[a], Fiorenza Cocchi[a,c], Olga S. Latinovic[a,d], Frank Denaro[e], Fabio Romerio[a,c], Mahmoud Djavani[a], Man E. Charurat[a,c], Joseph L. Bryant[a,f], Hervé Tettelin[d,g], and Robert C. Gallo[a,c,1]

[a]Institute of Human Virology, School of Medicine, University of Maryland, Baltimore, MD 21201; [b]Department of Biochemistry and Molecular Biology, School of Medicine, University of Maryland, Baltimore, MD 21201; [c]Department of Medicine, School of Medicine, University of Maryland, Baltimore, MD 21201; [d]Department of Microbiology and Immunology, School of Medicine, University of Maryland, Baltimore, MD 21201; [e]Department of Biology, Morgan State University, Baltimore, MD 21251; [f]Department of Pathology, School of Medicine, University of Maryland, Baltimore, MD 21201; and [g]Institute for Genome Sciences, School of Medicine, University of Maryland, Baltimore, MD 21201

We isolated a strain of human mycoplasma that promotes lymphomagenesis in SCID mice, pointing to a p53-dependent mechanism similar to lymphomagenesis in uninfected p53^{−/−} SCID mice. Additionally, mycoplasma infection in vitro reduces p53 activity. Immunoprecipitation of p53 in mycoplasma-infected cells identified several mycoplasma proteins, including DnaK, a member of the Hsp70 chaperon family. We focused on DnaK because of its ability to interact with proteins. We demonstrate that mycoplasma DnaK interacts with and reduces the activities of human proteins involved in critical cellular pathways, including DNA-PK and PARP1, which are required for efficient DNA repair, and binds to USP10 (a key p53 regulator), impairing p53-dependent anticancer functions. This also reduced the efficacy of anticancer drugs that depend on p53 to exert their effect. mycoplasma was detected early in the infected mice, but only low copy numbers of mycoplasma DnaK DNA sequences were found in some primary and secondary tumors, pointing toward a hit-and-run/hide mechanism of transformation. Uninfected bystander cells took up exogenous DnaK, suggesting a possible paracrine function in promoting malignant transformation, over and above cells infected with the mycoplasma. Phylogenetic amino acid analysis shows that other bacteria associated with human cancers have similar DnaKs, consistent with a common mechanism of cellular transformation mediated through disruption of DNA-repair mechanisms, as well as p53 dysregulation, that also results in cancer-drug resistance. This suggests that the oncogenic properties of certain bacteria are DnaK-mediated.

DnaK | mycoplasma | p53 | DNA repair | cancer

About 20% of human cancers are caused by known infectious agents (1–3). Some, such as human T cell leukemia virus-1 (HTLV-1) and human papilloma virus (HPV), encode an oncogene, transforming cells directly. Others, although not directly transforming, encode genes which interfere with cellular regulatory mechanisms, such as the CagA protein of *Helicobacter pylori* (4, 5) and the NS5A protein of Hepatitis C virus (HCV) (6, 7), both antagonizing the p53 pathway. In another mechanism the microbe does not infect the cell which becomes transformed but alters the microenvironment (3) to favor DNA damage or inappropriate survival of nearby cells (e.g., HIV-1 and, again, HCV and *H. pylori*) (8–10). In recent years, studies of the composition of the human microbiome and the distribution of the microbiota have elucidated an array of complex interactions between prokaryotes and their hosts (11). A recent example is the association between *Fusobacterium nucleatum* and colorectal cancer (12–15). However, precise bacterial pathogen–cancer relationships and the mechanisms involved inducing neoplasia remain largely elusive, although several bacteria, by establishing persistent infections, can alter host cell cycles, affect apoptotic pathways, and stimulate the production of inflammatory substances

linked to DNA damage, thus potentially promoting abnormal cell growth and transformation.

Some mycoplasmas are particularly suspicious bacteria for involvement in oncogenesis. Although most are extracellular, some invade eukaryotic cells (16) and have been associated with some human cancers, including non-Hodgkin's lymphoma (NHL) (17), prostate cancer (18), and oral cell carcinoma (19) in HIV-seropositive subjects. In addition, it has been shown that persistent infection with *Mycoplasma penetrans* in a chemically immunosuppressed mouse model results in lower p53 and p21 expression in gastric mucosal cells (20). Moreover, in vitro infection of *Mycoplasma fermentans* subtype *incognitus* induces chromosomal alterations in both human prostate and murine embryonic cell lines, resulting in phenotypic changes leading to the acquisition of malignant properties in mouse and human cells, including loss of anchorage dependency and the ability to

---

Significance

We provide evidence here that (*i*) a strain of mycoplasma promotes lymphomagenesis in an in vivo mouse model; (*ii*) a bacterial chaperone protein, DnaK, is likely implicated in the transformation process and resistance to anticancer drugs by interfering with important pathways related to both DNA-damage control/repair and cell-cycle/apoptosis; and (*iii*) a very low copy number of DNA sequences of mycoplasma DnaK were found in some tumors of the infected mice. Other tumor-associated bacteria carry a similar DnaK protein. Our data suggest a common mechanism whereby bacteria can be involved in cellular transformation and resistance to anticancer drugs by a hit-and-hide/run mechanism.

MICROBIOLOGY

form colonies in soft agar and tumorigenicity in nude mice (21–23). Finally, the infection of different human cell lines (fibroblast, embryonic kidney, breast cancer, colorectal carcinoma) and mouse fibroblasts with several mycoplasmas (*M. fermentans*, *Mycoplasma arginini*, *Mycoplasma hominis*, and *Mycoplasma arthritidis*) inhibits p53 activity, and these mycoplasmas cooperate with Ras in oncogenic transformation, although the responsible bacterial protein has not been identified (24). Although their role remains unclear and controversial, and to date no direct carcinogenic role for any mycoplasma has been demonstrated in vivo, these findings are consistent with the notion that mycoplasmas may facilitate tumorigenesis and in some cases be directly involved in one or more stages of tumor causation.

Results

Mycoplasma Induces Lymphoma in Vivo. Given the frequent detection of *M. fermentans* in HIV-1–seropositive subjects (25) and its reported association with AIDS-related NHL (17), we evaluated the tumorigenicity of this mycoplasma in the context of immune deficiency. We used a strain of *M. fermentans* isolated at the Institute of Human Virology (IHV) from an HIV-1$^+$ cell line, about 0.5–1.5% different in nucleotide sequence from the mycoplasma prototypes (*SI Appendix, Materials and Methods* and Fig. S1 *A–C*). This mycoplasma strain was used to infect a SCID mouse model. The SCID phenotype (*Prkdc$^{-/-}$*) results from a defect in DNA repair caused by the lack of DNA-dependent protein kinase (DNA-PK). B and T cells do not mature because of the inability to recombine Ig and T cell receptor chains, respectively (26). The inability to join dsDNA hampers the ability of these lymphocytes to progress through the cell cycle and eventually leads to their p53-dependent apoptosis (27, 28). Consequently, these animals are deficient in B and T cells although some immature cells develop, particularly in the T cell lineage. Indeed, about 40–60% of SCID$^{prkdc-/-}$ mice develop T cell lymphoma at 32–48 wk of age. SCID$^{prkdc-/-}$ mice carrying an additional *p53$^{-/-}$* mutation develop T cell lymphomas at a faster rate (more than 90% by about 14 wk of age) (29), indicating that p53 provides a protective effect. Given both the association of mycoplasma with human tumors in vivo and the effect of mycoplasma on p53 in vitro (24), we infected nonobese diabetic (NOD)/SCID and CB17.SCID mice with our isolates of *M. fermentans* to test the hypothesis that this mycoplasma would accelerate lymphomagenesis by interacting with p53 in vivo. If this hypothesis were correct, we would expect transformed T cells to appear soon after infection. As a negative control, we used NOD.Cg-*Prkdc^{scid} Il2rg^{tm1Wjl}*/SzJ mice, also known as "NOD/SCID-γ" (NSG) mice, which do not express the PRKDC gene or the X-linked IL-2Rγ gene (30). These animals very rarely develop spontaneous T cell lymphoma even after sublethal irradiation, most likely because the lack of a functional IL-2 receptor further hampers T cell proliferation. Uninfected controls and infected NSG mice did not develop tumors during the time of the experiment (Fig. 1*A*). However, enlarged spleens, thymuses, and lymph nodes were apparent in the SCID mice as early as 8 wk following *M. fermentans* infection (Fig. 1 *B* and *C*). Histochemical analyses showed lymphoid cells infiltrating the organs of infected animals (Fig. 1*D* and *SI Appendix*, Fig. S2 *A–F*). To verify that the infiltrating lymphocytes causing organ enlargement were transformed, aliquots of single-cell suspensions from an enlarged lymph node of an *M. fermentans*-infected animal were injected i.p. into young (~6-wk-old) NOD/SCID mice. Extranodal tumors were detected as early as 2 wk after injection. Secondary tumor cells were phenotypically characterized by flow cytometry. These cells were CD4$^+$/CD8$^+$ CD3^{high} and CD4$^+$/CD8$^+$ CD3, showing the same phenotype as the cells detected in uninfected mice that developed spontaneous lymphomas at about 38–40 wk of age (*SI Appendix*, Fig. S3 *A–C*). Thus, the tumor cells appeared much earlier in the life span of the mycoplasma-infected animals,

indicating the occurrence of a transforming event(s) soon after mycoplasma infection (Fig. 1*A*). PCR analysis showed the presence of a very low copy number of mycoplasma DNA sequences in enlarged spleens and lymph nodes of infected mice and in secondary tumors composed of transformed cells originating from infected mice (*SI Appendix*, Table S1).

Our data are consistent with an anticipated lymphomagenesis induced by a reduction of p53 activity, similar to that previously described in SCID$^{prkdc-/-}$ mice carrying an additional *p53$^{-/-}$* mutation (29). Together with the presence of mycoplasma DNA sequences in some primary and secondary tumors, they indicate that cellular transformation most likely originated through a hit- and-hide/run infectious process. Our data are also consistent with two previous reports, one showing the reduction of p53 and p21 potentially facilitating malignant transformation in a chemically immuno-suppressed mouse model infected by mycoplasma (20), and the other showing in vitro that infection of several rodent and human cell lines with *M. fermentans*, *M. arginini*, *M. hominis*, and *M. arthritidis* suppressed the transcriptional activity of p53 (24). This impairment resulted in lack of transcription of p21 following treatment with 5-fluorouracil (5-FU), a thymidylate synthase inhibitor that causes DNA damage and eventually results in the activation of p53. Damaged cells proliferated and did not undergo apoptosis at the same rate as uninfected cells, raising the possibility that transforming events could accumulate in these cells (24). The mycoplasma protein(s) responsible for the effect were not identified.

Mycoplasma DnaK Binds USP10 and Impairs p53-Dependent Functions. To identify which *M. fermentans* protein is responsible for reducing p53 activities, pull-down experiments were conducted on mycoplasma-infected HCT116 cells (a colorectal carcinoma cell line) using an anti-p53 monoclonal antibody. Following infection, recovered products were characterized by HPLC MS and micro-sequencing (*SI Appendix, Materials and Methods* and Table S2). Several mycoplasma-specific proteins were identified, including DnaK, which is the prokaryotic heat shock protein Hsp70, a stress-induced protein. Eukaryotic organisms express several slightly different Hsp70 proteins when subjected to stressful conditions, and the overexpression of some increases the transformation of several human cell types (31, 32). Suppression of Hsp70 expression by antisense Hsp70 cDNA inhibits tumor cell proliferation and induces apoptosis (33).

While bacterial DnaK proteins form a family with diversity of amino acid sequences, they are a central hub in prokaryotic protein-interaction networks (34). For instance, DnaK from *Escherichia coli* interacts with human and murine p53 (35–38) and increases p53 activity, although the meaning of these interactions is not clear (39).

To analyze the effect of mycoplasma DnaK on p53-dependent cellular pathways, HCT116 cells transfected with codon-optimized DnaK (*SI Appendix*, Fig. S4) were treated with Nutlin-3, which releases active p53 from its natural ligand and inhibitor MDM2 (Mouse double minute-2) (40). The expression of p53, p21, Bax (Bcl-2–associated X protein), and PUMA (P53 up-regulated modulator of apoptosis) was then analyzed up to 16 h after transfection. Reduced levels of p21, Bax, and PUMA were observed when DnaK-transfected HCT116 cells were treated with Nutlin, as compared with control cells (Fig. 2*A*), indicating that mycoplasma DnaK was impairing p53 functions. Of note, when the same experiments were performed to investigate the effect of *E. coli* DnaK, we observed the opposite effect, i.e., an increase in p53 activity (*SI Appendix*, Fig. S5), as also previously reported by others (39).

p21 is a cyclin-dependent kinase inhibitor that is transcriptionally up-regulated by p53 in response to DNA damage, hypoxia, and nucleotide pool perturbation, leading to inhibition of retinoblastoma phosphorylation and cell-cycle arrest at the G1-to-S transition (41). We therefore investigated whether the previously observed reduced amounts of p53 and p21 (Fig. 2*A*) correlated
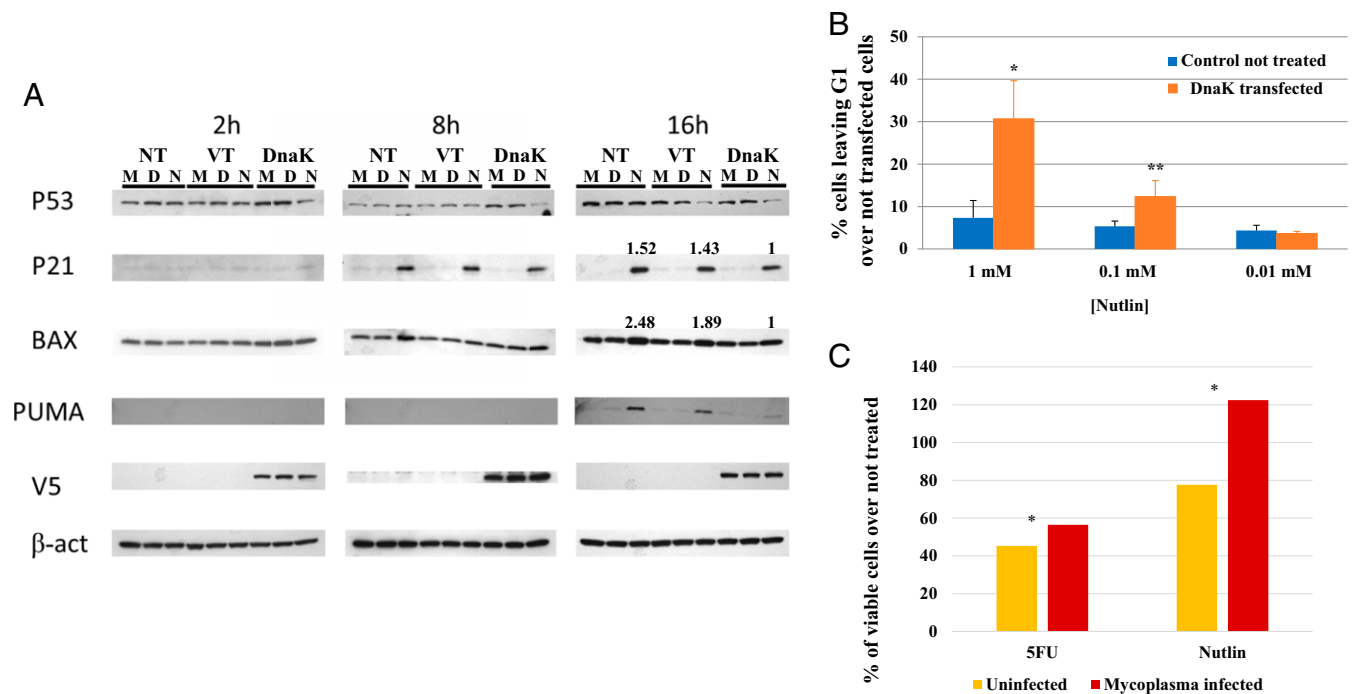
Fig. 1. Mycoplasma infection induces tumorigenesis in SCID mice. (*A*) Mycoplasma infection in SCID mice. An inverted Kaplan–Meyer formula was used to generate a plot of the time to tumor development. CB17.SCID (*n* = 18) and NOD/SCID (*n* = 12) mice were infected with a strain of *M. fermentans* isolated at the IHV. The experiments were carried out for about 19–20 wk after infection, until the animals reached an age of about 27 wk. Of the 30 infected animals, 12 (eight CB17.SCID and four NOD/SCID) mice developed tumors by 27 wk of age, starting at about 8 wk after infection. The CB17.SCID animals belonged to a colony maintained in our animal facility under pathogen-free conditions. NOD/SCID and NSG mice were obtained from the Jackson Laboratory. Young animals (about 6 wk old) were infected by i.p. injection with mycoplasma (10^7 pfu). Tumor development was observed in animals infected with mycoplasma grown in either aerobic or anaerobic conditions. As early as 7 wk post infection the spleen and lymph nodes were enlarged in animals infected with mycoplasma. In some animals tumor cells colonized the vestigial thymic area, and necropsy showed an enlarged tumor mass. About 30% of the animals died of wasting within 30 wk of infection. Age-matched uninfected CB17.SCID (*n* = 9) and NOD/SCID (*n* = 9) animals were kept in adjacent cages as controls. Control, uninfected CB17.SCID mice had a lifespan of about 40–50 wk, and NOD/SCID mice had a lifespan of 38–45 wk. Only one CB17.SCID mouse developed a spontaneous tumor at about 26 wk of age. Spontaneous T cell lymphoma was observed in more than 40% of both the CB17.SCID animals and the NOD/SCID animals after 33 wk of age. As a further control, we used NSG mice, which are resistant to lymphoma development even after sublethal irradiation treatment. None of the infected NSG animals (*n* = 8) developed tumors during the time of the experiment. In some experiments (*n* = 10 mice) we also used the prototype *M. fermentans* PG18 grown under standard conditions. Seven animals died of wasting within 30 wk after infection, and none of the remaining animals developed lymphoma. Eight animals were injected with nonviable mycoplasma, and none developed lymphoma up to 28 wk of age (see also *Materials and Methods*). (*B*) Splenomegaly and enlarged lymph nodes in mycoplasma-infected mice that developed tumors. Spleens from mycoplasma-infected animals and uninfected animals were collected and compared to determine size increase. Uninfected spleens showed very little variation in size and were considered as references in comparing the size of spleen from infected animals. (*C*) Analysis of spleens from a total of seven infected animals and five uninfected animals. Error bars indicate SD. *P < 0.01; Student's *t* test. (*D*) Tumor infiltration of mycoplasma-infected mice. (*1*) Image of an H&E-stained section of a peripheral lymph node showing increased cellularity of tumor infiltration. (Magnification; 10×.) Increased vascularity is indicated by numerous slits. (*2*) Image of an H&E-stained section of tumor infiltration of a peripheral lymph node. (Magnification; 20×.) Note the prominent follicular hyperplasia with a poorly defined medullar zone. (*3*) Image of an H&E-stained section of the spleen with prominent red pulp showing increased cellularity of tumor infiltration. (Magnification; 10×.) Increased vascularity is indicated by numerous slits. (*4*) Image of an H&E-stained of a spleen with a tumor infiltration. (Magnification; 10×.)

with changes in the cell cycle. As expected, a marked increase in cells leaving G1 was observed in HCT cells treated with Nutlin and then transfected with mycoplasma DnaK (Fig. 2*B*).

These data indicate that resistance to anticancer drugs that work at least in part by p53 activation may occur with infection with some mycoplasmas. To test this hypothesis, we infected cells treated with two drugs currently used in cancer treatment: 5-FU and Nutlin. As expected, mycoplasma infection resulted in resistance to these anticancer drugs (Fig. 2*C*).

However, we failed to verify a direct interaction between p53 and transfected DnaK from *M. fermentans*. This suggests that DnaK may reduce p53 activity by binding to p53 with low affinity or that it binds to a regulatory protein(s) complex that includes p53. Consequently, we determined the cellular proteins interacting with DnaK by performing a pull-down experiment of DnaK-transfected cells. Several proteins were identified (Table 1).

USP10 (ubiquitin carboxyl-terminal hydrolase protein-10) is one of the most important regulators of p53. By removing conjugated ubiquitin from target proteins, including p53, USP10 increases p53 stability in unstressed cells. This process is very important during the DNA-damage response, when USP10 translocates to the nucleus and deubiquitinates p53, stabilizing it and thus regulating its response to DNA damage (42). We first confirmed the interaction between DnaK and USP10 by immunoprecipitation studies (Fig. 3*A*). Next, we performed immunoblotting studies of cells treated with 5-FU and cotransfected with two vectors, one expressing USP10 and the other expressing DnaK. The presence of DnaK dramatically increased the amount of ubiquitinated p53 (Fig. 3*B*), indicating that p53 is less stable in the presence of DnaK. Finally, to verify this effect on the stability of p53, cells treated with 5-FU and cycloheximide, a protein-synthesis inhibitor, were transfected with DnaK, and the p53 levels were measured over a short period of time

Fig. 2. DnaK negatively affects p53 activities, and mycoplasma infection reduces the effect of anticancer drugs. (*A*) DnaK reduces p53-associated activity in HCT116 cells. Levels of p53, p21, Bax, and PUMA proteins were analyzed in control and vector- and DnaK-transfected cells at different time points (2, 8, and 16 h). DnaK expression was verified using the anti-V5 antibody. β-act, β-actin; D, DMSO; DnaK, DnaK transfected; M, medium; N, Nutlin; NT, not transfected; VT, vector transfected. Band intensity was measured by densitometric analysis. Numbers above bands indicate the fold increase above the level of Nutlin-treated DnaK-transfected cells, normalized for the levels of β-actin. (*B*) DnaK increases cell-cycle progression. HCT116 cells were transfected with a DnaK-expressing vector and subsequently analyzed for cell-cycle progression. Data were collected 16–24 h after transfection. Results represent the mean and SDs of five different experiments. *$P < 0.02$; **$P < 0.05$; Fisher's exact t test. (*C*) Mycoplasma infection reduces the effect of the chemotherapeutic drugs 5-FU and Nutlin. HCT116 cells were infected with mycoplasma. Results are expressed as percent cell viability over control (uninfected cells in medium alone were considered as 100%). Mean difference is shown. *$P < 0.001$ calculated using Poisson regression.

(4 h). The half-life of p53 was decreased in cells treated with 5-FU and transfected with DnaK as compared with the mock-transfected cells (Fig. 3*C*). Taken together, our results indicate that DnaK binding to USP10 prevents its deubiquitinating activity, thus reducing p53 stability and its anticancer functions and the cellular response to some anticancer drugs.

Mycoplasma DnaK Hampers Activity of PARP1, a Critical Protein Involved in DNA Repair. Another important protein listed in Table 1 is poly-ADP ribose polymerase-1 (PARP1), one of the most studied members of the family of PARP proteins. PARP1 is involved in the recognition and subsequent repair of DNA lesions (43–45). Following the interaction with damaged DNA, PARP1 activity is increased dramatically, resulting in PARylation of several proteins, including itself, histones, topoisomerase 1 (TOP1), DNA-PK, and others (46). This causes the recruitment to the damaged site of factors involved in double- and single-strand break repair, base-excision repair, and nucleotide excision repair (47–49). Failure to repair DNA damage properly usually results in

apoptosis to avoid the accumulation of DNA damage that ultimately could lead to cellular transformation.

We first verified that DnaK could immunoprecipitate PARP1 (Fig. 4*A*). Next, we wanted to evaluate the effect of DnaK on the catalytic activity of PARP1. A colorimetric assay was used to measure the inhibitory effect of DnaK on PARP1's ability to PARylate histone immobilized on plates. A sharp decrease in histone PARylation was observed in the presence of DnaK, indicating that it hampered PARP1 catalytic activity (Fig. 4*B*). We also confirmed immunoprecipitation by DnaK of another protein important for DNA repair, DNA-PK$_{CS}$, the catalytic subunit of DNA-PK (Fig. 4*C*). Recruited to the site of damage by the heterodimer KU70/80 and forming a complex with other proteins, DNA-PK$_{CS}$ is required for nonhomologous end joining in both dsDNA repair and V(D)J recombination (50, 51). For effective and proper functioning, the spatial and temporal arrangement of these important multiprotein complexes must be very tightly controlled and regulated. The interaction of DnaK with two proteins important for the recognition of DNA damage and repair, resulting in decreased PARP1 catalytic activity, would

Table 1.   DnaK binds to proteins involved in critical cell pathways

Cellular proteins interacting with DnaK (immunoprecipitation analysis)	Protein function
PARP1	DNA repair
DNA-PKcs	DNA repair
USP10	Deubiquinitates and regulates p53 stability
DNAJA1 (HSP40 family)	HSP70 activator

Proteins found to immunoprecipitate with DnaK are listed. Proteins analyzed but found not to immunoprecipitate are BRCA2, HSP90b1, p53, HSP70, KU86, SP1, DDB1, ING1, DNAJA2, and DNAJB1.
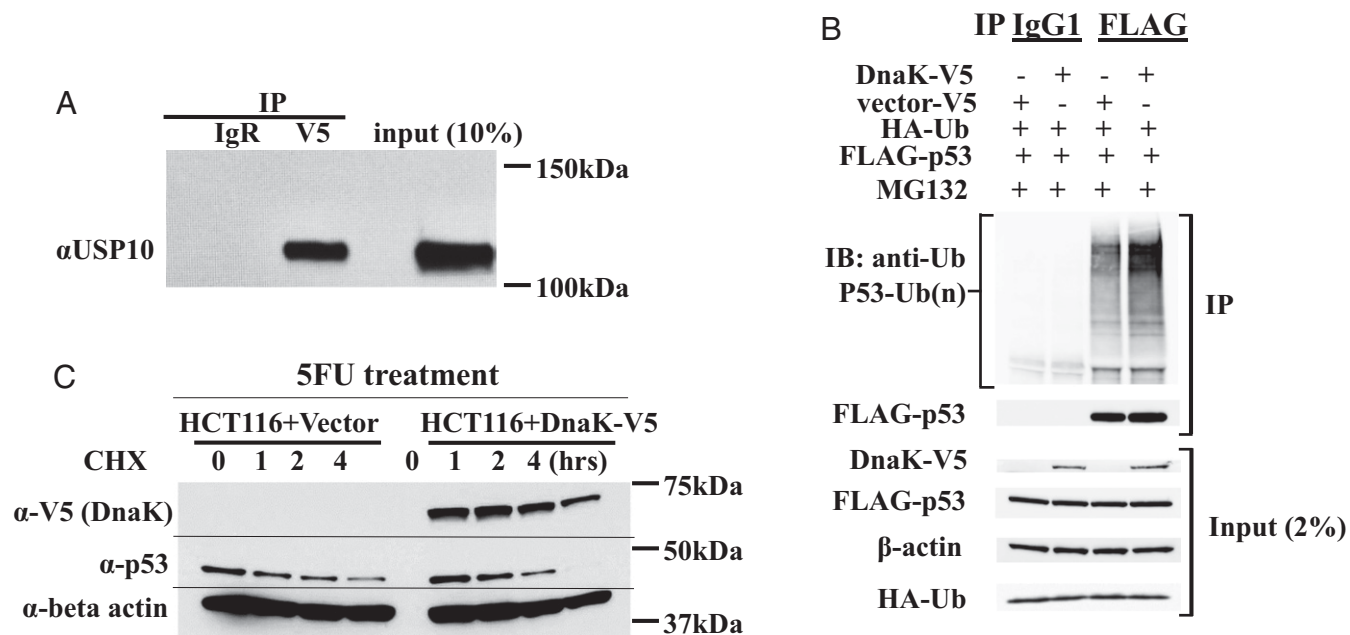
Fig. 3. DnaK Immunoprecipitates USP10 and reduces the stability of p53 upon DNA damage. (*A*) Immunoprecipitation analysis shows binding of DnaK to USP10. HCT116 cells were transfected with DnaK-V5, and immunoprecipitation was performed using anti-V5 antibody and IgR [antibody isotype control (rabbit)]. After washing, the immunoprecipitated products were loaded on an acrylamide gel as described in *Materials and Methods*. αUSP10, anti-USP10 antibody. (*B*) DnaK induces p53 ubiquitination. HCT116 cells were cotransfected with DnaK-V5 together with HA-Ubiquitin (HA-Ub) and Flag-p53 expression vectors. Empty V5-vector was used as a negative control. Cells were treated with the proteasome inhibitor MG132 for 5 h before harvest. Flag-p53 and IgG isotype control immunoprecipitates (IP) or whole-cell lysates (Input) were immunoblotted with anti-Flag and anti-HA. Input lysates were also immunoblotted with anti-V5 and anti–β-actin antibodies. The immunoblot is representative of two independent experiments. (*C*) DnaK regulates p53 stability. CT116 cells transfected with DnaK-V5 or the control vector were treated with cycloheximide (CHX) (0.1 mg/mL) and were harvested at time points 0, 1, 2, and 4 h. Cell lysates were then blotted with anti-V5 (Top panel), anti-p53 (Middle panel), and anti–β-actin (Bottom panel) antibodies.

likely lead to apoptosis or to the accumulation of DNA damage, thereby increasing the probability of cellular transformation (52). Mice lacking PARP1 exhibit high levels of sister chromatid exchange (53, 54) and increased chromosome aberrations, including fusions, breaks, and telomere shortening (55), and double-mutant DNA-PK/PARP-deficient mice develop T cell lymphomas at high frequency (56).

The chaperone activity of HSP70/DnaK is controlled by cycles of ATP binding and hydrolysis (57). Although DnaK itself is a weak ATPase, its interaction with the cochaperone DNAJ proteins (members of the HSP40 family) increases ATPase activity, promotes binding with target proteins, and accelerates the protein-folding activity of HSP70/DnaK (58). To determine whether intracellular mycoplasma DnaK has possible chaperone activity, we verified its binding with a human DNAJ protein, DNAJ1A1, previously identified in protein sequencing of DnaK-bound cellular proteins (Table 1). Immunoprecipitation studies confirmed that DnaK is able to bind human DNAJ1A1 (Fig. 4*D*). This could indeed indicate that, once in the intracellular compartments, bacterial DnaK becomes functionally active by exploiting the cellular cochaperone DNAJA1. This suggests that DnaK negatively affects eukaryotic proteins by three possible mechanisms: (*i*) direct binding of the proteins and thus hampering their ability to form proper functional complexes; (*ii*) direct binding and improperly folding of the target proteins, thus rendering them inactive and/or targeting them for degradation; and (*iii*) binding to complex(es) of proteins and altering their effectiveness.

Exogenous Mycoplasma DnaK Is Taken Up by Bystander Cells. Bacteria can translocate proteins into eukaryotic cells either by attaching to the outside of the cellular membrane or by invading the cell (59, 60). In addition, prokaryotic and eukaryotic membrane-localized HSP70 proteins may be released into the surrounding microenvironment and then translocate into the cytoplasm of nearby cells

(61–65). Given these properties of HSP70 proteins, we tested the ability of exogenous mycoplasma DnaK to be taken up by bystander cells. A recombinant protein, DnaK-V5, was constructed and added to HCT116 cells. After 24 h, exogenous mycoplasma DnaK-V5 was localized in several cellular compartments, including cytoplasm, the perinuclear membrane, and nucleus (Fig. 5 *A* and *B*). These results expand our knowledge from previously published data (64) about the ability of certain cells to bind and internalize HSP70s. The cellular uptake of DnaK-V5 was visualized using the Z-stacks option, in which the gallery of images shows the clear presence of the protein inside the cells (Fig. 5 *A* and *B*). The lower image in the right corner of Fig. 5 *A* and *B* is a 3D presentation based on the collected Z-stacks of corresponding gallery of images. Two negative controls that were imaged under the same conditions are presented in Fig. 5 *C* and *D*. In conclusion, our data demonstrate that exogenous mycoplasma DnaK is taken up by uninfected cells, and this uptake may result in the impairment of pathways relevant for critical cellular functions, thereby altering the control of cell growth in uninfected cells.

Amino Acid Analysis Reveals Similarities Among Bacterial DnaKs Associated with Human Cancers. Several bacteria have been associated with certain human cancers. The most notable is the association of *H. pylori* with gastric cancer (66). Others are *F. nucleatum*, mainly associated with colorectal cancer (12–14), *Chlamydia trachomatis*, associated with cervical cancer (67–69), and some mycoplasma associated with NHL (17), prostate cancer (18), and oral cell carcinoma (19). The mechanisms of cellular transformation are largely unknown, although at least one has been proposed for *H. pylori*, whereby the CagA protein alters the p53 pathways (4). We note that, in common with mycoplasma, these bacteria have the ability to invade cells and, like *H. pylori*, disseminate key proteins into the cellular cytoplasm and thus possibly transform the cell. Given the
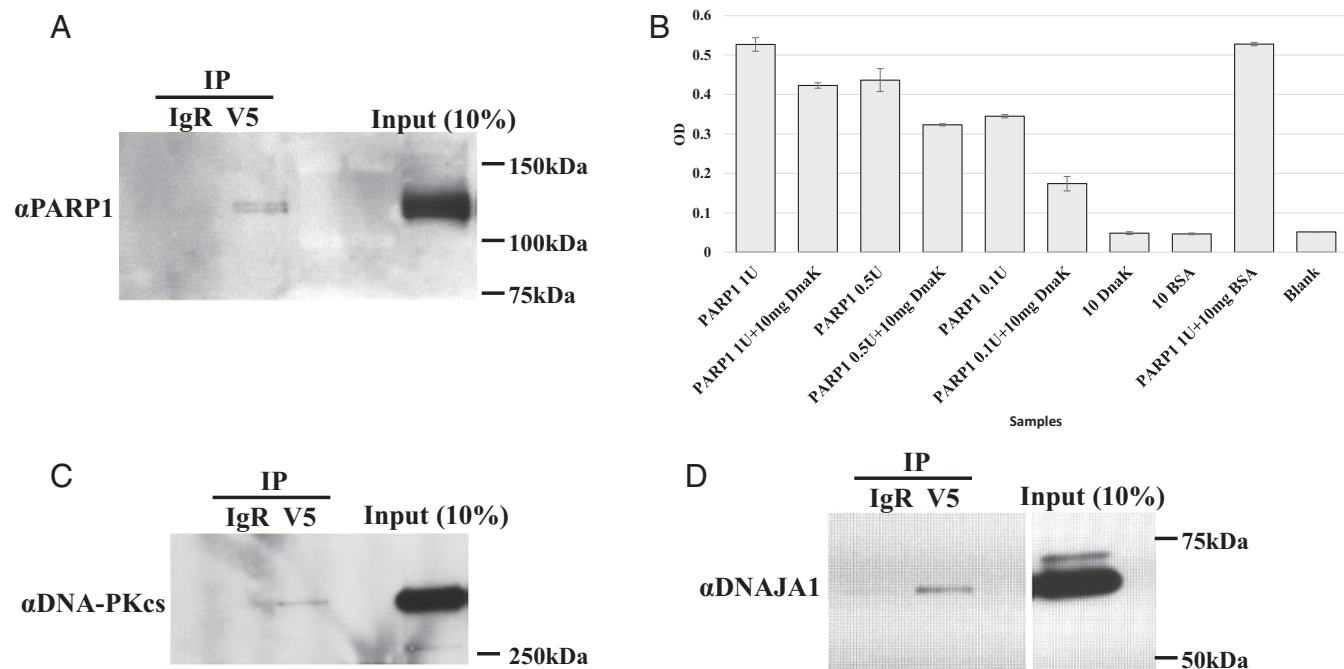
MICROBIOLOGY

Fig. 4. Interaction of DnaK with proteins implicated in the DNA-repair pathway and with DNAJA1. HCT116 cells were transfected with DnaK-V5, and immunoprecipitation was performed using anti-V5 antibody and antibody isotype control (Rabbit) (IgR). After washing, the immunoprecipitated products were loaded on an acrylamide gel as described in *Materials and Methods*. (*A*) Immunoprecipitation analysis shows binding of DnaK to PARP1. αPARP1, anti-PARP1 antibody. (*B*) Measurement of the catalytic activity of PARP1 shows reduced histone PARylation in the presence of DnaK. Purified PARP1 and DnaK were incubated together, and PARP1 activity was subsequently analyzed according to the protocol described in *Materials and Methods*. (*C*) Immunoprecipitation analysis shows binding of DnaK to DNA-PK$_{CS}$. αDNA-PK$_{CS}$, anti–DNA-PK$_{CS}$ antibody. (*D*) Immunoprecipitation analysis shows binding of DnaK to DNAJA1. αDNAJA1, anti-DNAJA1 antibody; IP, immunoprecipitation; V5, tag for DnaK.

oncogenic properties of mycoplasma DnaK, we compared the DnaKs from cancer-associated bacteria to highlight any similarities that might potentially play a role in mechanisms of cellular transformation. Available amino acid sequences of DnaKs were aligned, and Mega 7.0.20 software (70) was used to create a phylogenetic tree (Fig. 6). We note that the mycoplasma DnaK amino acid sequence is strikingly close to those of *H. pylori*, *F. nucleatum*, and *C. trachomatis*, bacteria consistently associated with different types of human cancers. Conversely, all these DnaKs are phylogenetically distinct from *E. coli* DnaK, which does not decrease p53 functions (Fig. 6) (35–39). Thus it appears that other bacteria able to establish intracellular infection and associated with cancers carry a DnaK that is likely able to interact, to varying degrees, with cellular proteins implicated in critical cellular pathways and thereby can contribute to cellular transformation events and possibly reduce the effect of anticancer drugs through the same mechanism(s) as mycoplasma DnaK.

Discussion

A growing number of bacteria have been associated with human cancers. While thus far *H. pylori* is the only bacterium for which clear epidemiological data support a causal association (66) and for which a detailed molecular mechanism is now proposed (4), studies of other bacteria, including *F. nucleatum* (12–14), *C. trachomatis* (67–69) and mycoplasmas (17–23), strongly support their role as leading candidates with oncogenic properties. While the accumulation of DNA damage and the hampering of p53 activity play a major role in driving transformation, the molecular mechanisms whereby these bacteria dysregulate cellular pathways are largely unknown.

We show here that a specific strain of mycoplasma DnaK promotes lymphomagenesis in a murine in vivo model. These animals (*Prkdc*$^{-/-}$) have a defect in a DNA-repair gene, DNA-PK, and the mice ultimately develop spontaneous T cell lymphoma

(26, 27). Previous studies have shown that SCID$^{prkdc-/-}$ mice with an additional *p53*$^{-/-}$ mutation develop T cell lymphomas earlier (29) and that this model is suitable for detecting oncogenic agents affecting DNA repair and p53 activities (28). According to our data, mycoplasma DnaK infection causes a series of events leading to cell transformation at a faster rate. Our data are in accordance with previous in vitro and in vivo studies that highlighted the oncogenic properties of mycoplasma DnaK (20–24), although the precise molecular mechanism(s) has not been identified. We show here that DnaK, a bacterial chaperone protein belonging to the HSP70 family, interacts with several human proteins, namely USP10, PARP1, and DNA-PK$_{CS}$, involved in important cellular pathways. Based on our data, we hypothesize that the presence of bacterial DnaK protein inside the cell, interacting and hampering the function of cellular proteins critical for an effective DNA repair (PARP1 and DNA-PK$_C$), could lead to the accumulation of DNA damage. At the same time, the interaction of DnaK with USP10 reduces p53 activity, preventing its anticancer effectiveness. Reducing the efficacy of these two cellular pathways, which are critical for the detection, repair, and prevention of DNA damage propagation, would greatly increase the chances of cellular transformation following DNA breaks and chromosomal rearrangements caused by ionizing agents, chemicals, and factors present in the microenvironment (3). It would be of interest to study the possible interaction(s) of DnaK with components of the DNA mismatch repair system, since errors originating from spontaneous mutations constitute a great proportion of transformation events (71).

The mycoplasma DnaK DNA sequence was also found at a very low copy number in some of the primary and secondary tumor samples, pointing to a hit-and-hide/run mechanism of cellular transformation following bacterial infection. According to this hypothesis, once the cell is invaded, the expression of
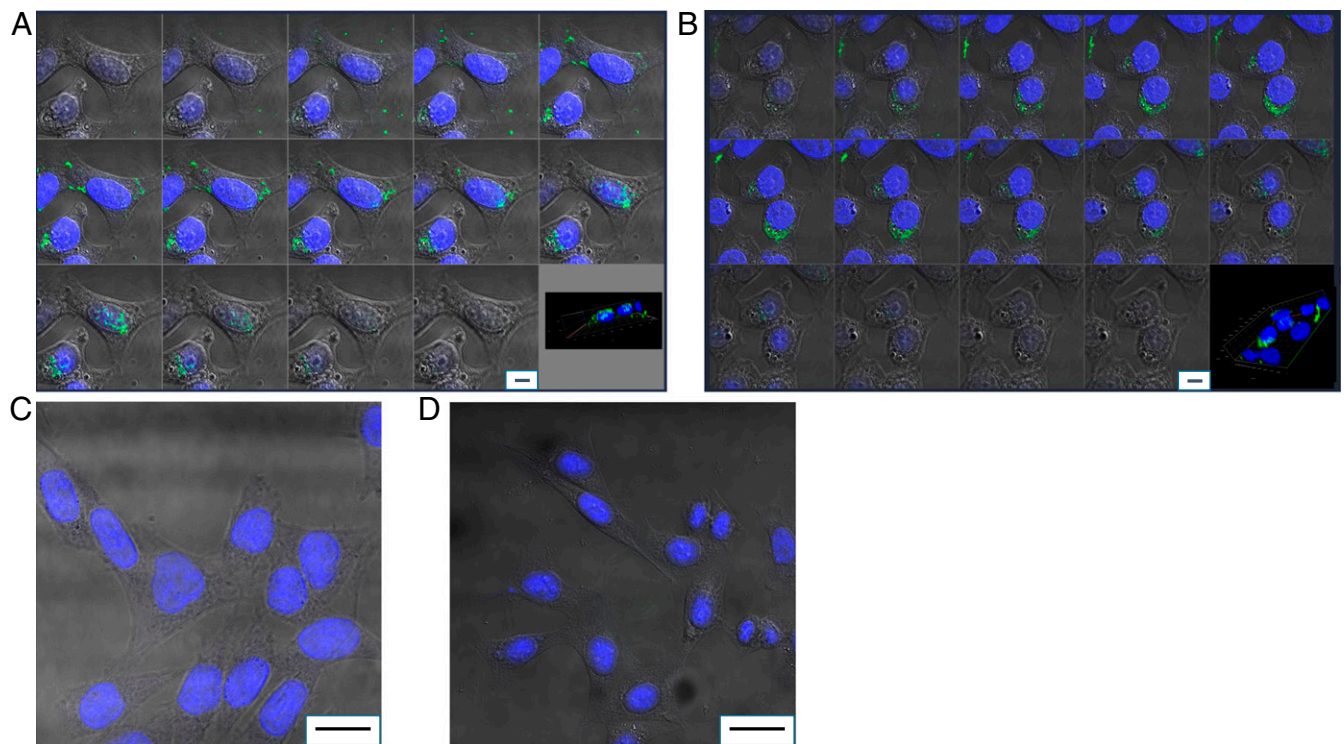
Fig. 5. Intracellular uptake of exogenous DnaK-V5 by mycoplasma-free HCT116 cells. Confocal images of exogenous DnaK-V5 protein of *M. fermentans* in HCT116 cells treated or not treated with DnaK-V5 protein. The figures show the collected Z-stacks of the corresponding gallery of images, each presenting a 0.5-μm-thick slide. A mouse monoclonal antibody, anti-V5, was used for primary labeling, and a FITC fluoresce-labeled antibody was used for secondary labeling. (*A*) Nuclear localization. (*B*) Perinuclear localization. (*C*) Primary and secondary antibodies alone without DnaK-V5 protein. (*D*) Negative control: no antibodies and no protein. DAPI staining was used for nuclei detection. *Insets* in the lower right corners of *A* and *B* show a corresponding constructed 3D presentation of the protein uptake. (Scale bars: 5 μm in *A* and *B*; 20 μm in *C* and *D*.)

DnaK would lead to cellular transformation (hit). At this point, only a few copies of the bacterium's DNA can be found in the tumor (hide), or the bacterium may not leave any trace of its presence (run). DnaK could exert these negative effects both in infected cells and in nearby uninfected cells, once this bacterial protein is released by the infected cells and taken up by the nearby cells. We speculate that, once in the cytoplasm, DnaK could hamper a number of cellular pathways, perhaps even in the absence of continued bacterial infection. We also compared DnaK amino acid sequences among several bacteria frequently associated with human cancers. The similarities of these DnaKs suggest the possibility of a broad mechanism of tumorigenesis which involves DnaK.

Our data may be clinically relevant for several reasons. First, several human cancers result, at least in part, from events leading to failures in DNA repair, which may be heightened by the presence of certain DnaK proteins in the cell. This would indicate that the origin of cancers might involve bacteria more frequently than currently appreciated. Second, it is conceivable that the DnaK of some bacteria could counteract the efficacy of compounds such as 5-FU or Nutlin used in the treatment of some cancers, which depend upon increased p53 activity for their activity. It is thus obviously of biological interest and potential therapeutic relevance to verify these findings in broader studies in humans and to understand the physical basis and the mechanism(s) responsible for reduced activities and levels of critical cellular pathways.

Materials and Methods

Animals. All animal experiments were approved by the University of Maryland School of Medicine Institutional Animal Care and Use Committee. Female NOD/SCID and NOD/SCID-γ (NSG) mice were obtained from the Jackson Laboratory. The mice are designated as "Prkd scid/J." These mice carry

several mutations that affect the immune system. Female CB17.SCID mice belonged to a colony maintained in our animal facility under pathogen-free conditions. At about 6 wk of age, 30 animals were injected with the mycoplasma strains isolated at the IHV (10^7 pfu per animal in 500 μL of 1× PBS) as described in *SI Appendix*. Additionally, 10 animals were injected with the *M. fermentans* PG18 strain, and 8 animals were injected with an aliquot of nonviable mycoplasma. (Mycoplasma was heat-inactivated at 60 °C for 2 h, and nonviability was determined after retesting the same aliquots and verifying lack of growth.) Both CB17.SCID and NOD/SCID mice develop thymic lymphomas at a very high rate (more than 40%) at around 8 mo of age. We kept 18 uninfected animals as controls to verify the development of spontaneous lymphoma. As a further control, we injected eight NSG mice,
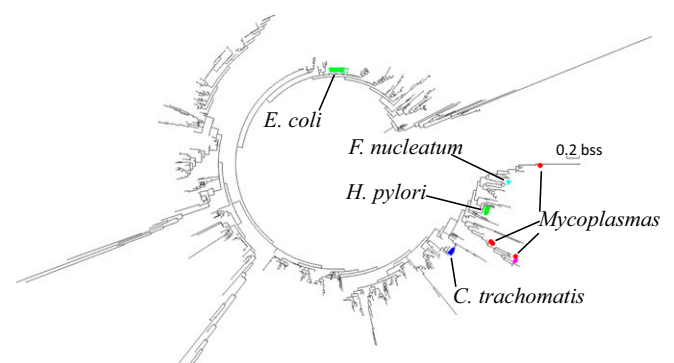

Fig. 6. Phylogenetic analysis of bacterial DnaKs. Published bacterial amino acid DnaK sequences were used to construct this tree using MEGA 7.02.20 software (*SI Appendix*, ref. 3). In addition to DnaKs from several strains of *E. coli*, other DnaKs from intracellular pathogens currently associated with some human cancers are indicated. bss, base substitutions per site.

which rarely develop spontaneous lymphomas. All animals were kept in Micro-Isolator caging systems under a controlled barrier system to avoid any contamination. A control group was injected with sterile water and housed under the same conditions. At necropsy, all tissues were collected and placed in 10% formalin and later were processed, stained with H&E, and reviewed by a pathologist blindly.

At the end of 3–6 wk we noted that the majority (7/10) of the NOD/SCID animals injected with PG18 suffered from pronounced weight loss and emaciation. Necropsy examination of the animals showed severe wasting and some mottling of the kidney. Histological examination showed acute to chronic inflammation in the lungs, kidney, liver, and joints. Some animals displayed little to no sickness until about 12 wk of age, at which time they displayed some weight loss and the slow development of dyspnea (difficult breathing). On gross examination, the thymus area in some animals was enlarged with a tumor-like homogenous mass taking up a large portion of the chest cavity, and there was enlargement of the spleen, liver, and lymph nodes in the mesentery and peripheral areas. Histologically, the tumor mass was a homogenous lymphoblastic infiltration with highly mitotic figures (Fig. 1D and *SI Appendix*, Fig. S2 A–F). Tumor invasion included the spleen, lymph nodes, kidneys, and brain. There was no tumor development in the NSG mice or the control mice. The eight animals injected with aliquots of nonviable *Mycoplasma* failed to develop tumors by 28 wk of age.

Western Blot Analysis. For Western blot analysis, cell monolayers were detached by scraping, washed in cold PBS, and solubilized in RIPA lysis buffer (Sigma) in the presence of protease inhibitors (Sigma). The amount of extracted protein was measured by the Bradford assay (Bio-Rad). Thirty micrograms of protein was resolved by SDS/PAGE, transferred to PVDF membrane (Bio-Rad), and probed with anti-p53 (Santa Cruz), anti-p21 (Abcam), anti-Bax (Cell Signaling), anti-PUMA (Calbiochem), anti-V5 (Invitrogen), and anti–β-actin (Cell Signaling) antibodies. Blots were incubated with a secondary HRP-conjugated antibody (Santa Cruz), developed using an ECL chemiluminescent substrate kit (Amersham Bioscience), and exposed to Kodak X-ray film.

Immunoprecipitation. For the immunoprecipitation experiments, detailed protocol and reagents are provided in *SI Appendix, Materials and Methods*.

HPLC Analysis and Sequencing of Proteins. Following immunoprecipitation, the gel pieces from the band were each cut into three slices, transferred to a siliconized tube, and washed in 200 μL of 50% methanol. The gel pieces were dehydrated in acetonitrile, rehydrated in 30 μL of 10 mM dithiothreitol in 0.1 M ammonium bicarbonate and were reduced at RT for 0.5 h. The DTT solution was removed, and the sample was alkylated in 30 μL of 50 mM iodoacetamide in 0.1 M ammonium bicarbonate at RT for 0.5 h. The reagent was removed, and the gel pieces were dehydrated in 100 μL of acetonitrile. The acetonitrile was removed, and the gel pieces were rehydrated in 100 μL of 0.1 M ammonium bicarbonate. The pieces were dehydrated in 100 μL of acetonitrile, the acetonitrile was removed, and the pieces were dried completely by vacuum centrifugation. The gel pieces were rehydrated in 20 ng/μL trypsin in 50 mM ammonium bicarbonate on ice for 30 min. Any excess enzyme solution was removed, and 20 μL of 50 mM ammonium bicarbonate added. The sample was digested overnight at 37 °C, and the peptides that formed were extracted from the polyacrylamide in a 100-μL aliquot of 50% acetonitrile/5% formic acid. This extract was evaporated to 15 μL for MS analysis.

The LC-MS system consisted of a Thermo Electron Velos Orbitrap ETD mass spectrometer system with an Easy Spray ion source connected to a Thermo 3-μm C18 Easy Spray column (through precolumn). Seven microliters of the extract was injected, and the peptides were eluted from the column by an acetonitrile/0.1 M acetic acid gradient at a flow rate of 0.25 μL/min over 1.6 h (three bands per sample). The nanospray ion source was operated at 1.9 kV. The digest was analyzed using the rapid switching capability of the instrument acquiring a full-scan mass spectrum to determine peptide molecular weights followed by product ion spectra (20) to determine the amino acid sequence in sequential scans. This mode of analysis produces ~90,000 MS/MS spectra of ions ranging in abundance over several orders of magnitude. Not all MS/MS spectra are derived from peptides. The data were analyzed by database searching using the Sequest search algorithm.

Cell-Culture Experiments and Cell-Viability Assay. HCT116 cells (a colon carcinoma cell line) were obtained from ATCC. Cells were maintained in McCoy's 5A medium (Invitrogen) supplemented with 10% FBS. For the cell-viability assay HCT116 mycoplasma-infected cells or transfected cells were plated in 96-well plates at a density of 15,000 cells/cm². Treatments were performed

on the day of plating, and cells were harvested 48 h later. The LIVE/DEAD Viability/Cytotoxicity Kit (Invitrogen) was used to determine cell viability, following the manufacturer's instructions. In all experiments cell viability was calculated as a percentage relative to the control cultures. For infection experiments, HCT116 cells were infected with MF-I1 grown in aerobic conditions, 10^6 pfu per 10^6 cells. After 48 h cells were plated in 96-well plates at a density of 5,000 cells per well for the cell-viability assay or in 75 cm² at a density of 150,000 cells/cm² for protein analysis. On the day of plating, cells were treated with 20 μM 5-FU or 10 μM Nutlin-3 or a corresponding volume of DMSO as control. In some experiments cells were treated with 10 μM 5-FU or 5 μM Nutlin-3. Cells were harvested after 48 h for the cell-viability assay and after 16 h for protein assays. For experiments with mycoplasma DnaK, semiconfluent cell monolayers were first transfected with DnaK or with the vector control and then were plated at the density described above. For time-course experiments, transfected cells, vector-treated control cells, and nontransfected control cells were plated at a density of 150,000 cells/cm², treated with 20 μM Nutlin-3 or DMSO (vol/vol), and collected after 2, 8, 16, and 24 h.

Transfection. HCT116 cells were transiently transfected with the plasmid DNA using Lipofectamine 2000 (Invitrogen) following the manufacturer's protocol. Briefly, 25 μg of plasmid DNA containing the insert or without the insert (control) was added to Lipofectamine suspended in reduced serum medium (OptiMEM; Invitrogen) and then was added to subconfluent cultures of HCT116 p53$^{+/+}$ and HCT116 p53$^{-/-}$ cells and incubated overnight at 37 °C in the presence of OptiMEM medium. Transfected cells were trypsinized and replated for subsequent experiments.

Cell-Cycle Analysis. Transfected HTC116 cells were plated in six-well culture plates in the presence of serum-free McCoy's medium and incubated at 37 °C to allow cell-cycle synchronization. After overnight serum starvation, serum was added to the cells at a final concentration of 5% (vol/vol) with or without treatment with different concentrations (100, 10, and 1 μM) of Nutlin-3 (Sigma) or control DMSO, and cells were incubated for 0, 2, 8, 16, or 24 h. Following incubation, cells were collected by trypsinization, washed with ice-cold PBS, and used for staining with propidium iodide following the protocol described previously, with minor modifications (72). Briefly, washed cells were fixed with ice-cold 70% ethanol overnight at 4 °C. Fixed cells were washed again and resuspended in PBS containing 10 μg/mL propidium iodide (Sigma) and 20 μg/mL bovine RNase A (Roche Applied Sciences) in a 37 °C water bath for 45 min and were analyzed by flow cytometry. The cell-cycle status of cells was analyzed using FlowJo software (FlowJo).

ELISA-Based Assay for Detection of PARP1 Activity. The ability of DnaK to inhibit PARP1 enzyme activity was assessed using Trevigen's HT Universal Colorimetric PARP1 Assay Kit, following the manufacturer's instructions. Different concentrations of PARP1 were incubated with 10 μg of DnaK-V5 protein, as indicated, for 30 min on ice. The same units of PARP1 without DnaK-V5 and the highest amount of PARP1 were used with 10 μg of BSA as negative controls. A sample without enzyme was used as black control. The samples were then loaded in duplicate into a 96-well histone-coated plate and were incubated in the presence of biotinylated NAD and activated DNA for 1 h at 37 °C. The wells then were incubated first with HRP-Streptavidin (Sigma-Aldrich) for 1 h at room temperature and then with a colorimetric substrate, following two washes with 1× PBS+0.1% Triton X-100 and two washes with 1× PBS. Finally, the absorbance was measured with a 96-well plate reader with a 450-nm filter.

In Vitro Ubiquitination Assay. Ubiquitination of p53 was detected as described previously (73). Briefly, HCT116 cells were transiently transfected with DnaK-V5 or control vector, Flag-p53, and HA-ubiquitin expression plasmids. After 48 h the cells were treated for 5 h with 20 μM MG132 (Millipore) and then were lysed under non-denaturating conditions (Cell Signaling). Ubiquitin aldehyde (R&D) was added to the lysate to a final concentration of 1 μM. Lysates were precleared with 50 μL of protein G Dynabeads (Thermo Fisher) for 1 h at 4 °C with a rotator at 20 rpm. Anti-Flag antibody (Sigma Aldrich) was used to immunoprecipitate ubiquitinated p53 proteins, and mouse IgG1 (Sigma) was used as a control. Immunoprecipitated samples were resolved by SDS/PAGE (12% gel from Novex) and analyzed by Western blotting with anti-HA and anti-Flag (both from Sigma). To ensure correct protein expression and loading, input samples were immunoblotted with anti-V5 (Abcam), anti-Flag, anti–β-actin (Cell Signaling), and anti-HA. pcDNA3 flag p53 (Addgene plasmid no. 10838) was obtained from Thomas Roberts, Dana–Farber Cancer Institute, Harvard Medical School, Boston; pRK5-HA-Ubiquitin-WT (Addgene

plasmid no. 17608) was obtained from Ted Dawson, Johns Hopkins University, School of Medicine, Baltimore.

Cell Culturing and Immunofluorescent Labeling for Detection of DnaK-V5 Cellular Uptake. For the immunofluorescence analysis, samples were prepared as follows. HCT116 cells (1×10^4 cells per well cultured in McCoy medium supplemented with 10% FBS, L-glutamine, and 1%, penicillin/ streptomycin 1%) were seeded in a four-well polylysine-coated chambered coverglass (Thermo Fisher Scientific) and were treated with DnaK-V5 protein (80 μg/mL) for 24 h. Negative controls were not treated with DnaK-V5. After washing, cells were fixed with 4% paraformaldehyde for 15 min at 37 °C, washed with 1× PBS, permeabilized with 0.1% Triton X-100 in 1× PBS for 15 min at RT, washed again, and blocked with 1% BSA and 10% serum from the species. The secondary antibody was raised in normal goat serum in 1× PBS for 60 min at RT. Primary labeling used a mouse monoclonal antibody directed against the V5 tag of the recombinant DnaK protein from *M. fermentans*. Cells were incubated in a humid chamber at RT with a 1:200 dilution of the primary antibody, anti-*Mycoplasma*-DnaK-V5 (V5 Tag mouse monoclonal antibody; Thermo Fisher Scientific) for 2 h. After three washes in PBS, cells were then incubated with a 1:1,000 dilution of fluorescent dye-labeled secondary antibody (goat anti-mouse IgG FITC; Thermo Fisher Scientific) for 45 min at RT in the dark. Finally, cells were washed three times in PBS, and PBS was added before immunofluorescence analysis. To demonstrate antibody specificity, primary mouse Isotype control monoclonal antibody (Thermo Fisher Scientific) and IgG fluorescein-conjugated secondary antibody were used as negative control. DAPI staining (Sigma) was used for nuclei detection.

PCR Analysis. Tissues were disrupted and homogenized using a rotor-stator homogenizer, and total DNA was extracted with the DNeasy Blood and Tissue Kit (Qiagen). Fifty nanograms of DNA were subjected to real-time PCR using the iQ SYBR Green Supermix Kit (Bio-Rad) with the ABI PRISM 5700 sequence detection system. All reactions were run in triplicate. Primers were selected using the National Center for Biotechnology Information/primer-Blast program (https://www.ncbi.nlm.nih.gov/tools/primer-blast/) and were synthesized by Sigma-Aldrich: Insertion sequence (PCR was performed with the following protocol: incubation at 95 °C for 5 min, 35 cycles of 30 s at 95 °C, 30 s at 60 °C, and 45 s at 72 °C): forward 5′-TCCCTTTCTTGACATGCTTTG-3′ and reverse 5′-CGCCTAATTTAAGAATGGTTGG-3′, yielding a PCR product of 167 bp; DnaK 368–462 (PCR was performed with the following protocol: incubation at 95 °C for 5 min, 35 cycles of 30 s at 95 °C, 30 s at 69 °C, and 30 s at 72 °C): forward 5′-ACAATGCACAACGTGAAGCCACA-3′ and reverse 5′-TGCTAAAG-CAGCAGCAGTAGGTTCG-3′, yielding a PCR product of 94 bp; DnaK 367–716 (PCR was performed with the following protocol: incubation at 95 °C for 5 min, 35 cycles of 30 s at 95 °C, 30 s at 62 °C, and 45 s at 72 °C): forward 5′-GACAATGCACAACGTGAAGC-3′ and reverse 5′-TCAGCAGCAGCTTTTAGACG-3′, yielding a PCR product of 350 bp; DnaK 367–954 (PCR was performed with the following protocol: incubation at 95 °C for 5 min, 35 cycles of 30 s at 95 °C, 30 s at 62 °C, and 45 s at 72 °C): forward 5′-GACAATGCACAACGTGAAGC-3′ and reverse 5′-ACGTGTTGAACCACCAACAA-3′, yielding a PCR product of 587 bp;

DnaK 688–1069 (PCR was performed with the following protocol: incubation at 95 °C for 5 min, 35 cycles of 30 s at 95 °C, 30 s at 62 °C, and 30 s at 72 °C): forward 5′-GCAATGGCTCGTCTAAAAGC-3′ and reverse 5′-CTGCAAGAA-CAGCACCTTGA-3′, yielding a product of 381 bp; DnaK 1037–1508 (PCR was performed with the following protocol: incubation at 95 °C for 5 min, 35 cycles of 30 s at 95 °C, 30 s at 70 °C, and 30 s at 72 °C): forward 5′-TGGGTGCTGCAATTCAAGGTGC-3′ and reverse 5′-GCACGTTTTGCATCAGCTT-CACG-3′, yielding a product of 471 bp; R1 (123) (PCR was performed with the following protocol: incubation at 95 °C for 5 min, 35 cycles of 30 s at 95 °C, 30 s at 61 °C, and 30 s at 72 °C): forward 5′-TCGCAACTCTAGATGCAGGAT-3′ and reverse 5′-AAACGAGTTGCTTGTTCTGCT-3′, yielding a product of 106 bp; R2 (1164) (PCR was performed with the following protocol: incubation at 95 °C for 5 min, 35 cycles of 30 s at 94 °C, 30 s at 65 °C, and 45 s at 72 °C): forward 5′-ACGGCTTTTCCGTTTTTGTCTT-3′ and reverse 5′-TGCATCCATGAACCGTATCCA-3′, yielding a product of 106 bp; R3 (100) (PCR was performed with the following protocol: incubation at 95 °C for 5 min, 35 cycles of 30 s at 94 °C, 30 s at 61 °C, and 45 s at 72 °C): forward 5′-AGCAATGGCTTTTGGTGATGC-3′ and reverse 5′-TGCATTGGACAGGCAAACGA-3′, yielding a product of 532 bp; R4 (95) (PCR was performed with the following protocol: incubation at 95 °C for 5 min, 35 cycles of 30 s at 94 °C, 30 s at 61.5 °C, and 45 s at 72 °C): forward 5′-AGATGGGACATTAGACGGGA-3′ and reverse 5′-TCGCGAGGACTTACCAACAT-3′, yielding a product of 816 bp.

For cloning, PCR was performed with the same set of primers and conditions, and the number of cycles was increased to 41. Bands were cloned into the PCRII TOPO plasmid (Thermo Fisher Scientific), according to the manufacturer's protocol and were sequenced to confirm identity with the targeted mycoplasma sequence.

Statistical Analysis. Time to developing lymphomas was performed using inverted Kaplan–Meier (KM) estimates with the log-rank test. KM at-risk time was calculated based on a follow-up of 20 wk after injection; mice that died were censored at the time of death. Differences in the proportions or percentages were tested using Fisher's exact test. Differences in the means were tested using Student's *t* test. All statistical tests were two-sided. Poisson regression was used to calculate statistical significance in Fig. 2C.

1. White MK, Pagano JS, Khalili K (2014) Viruses and human cancers: A long road of discovery of molecular paradigms. *Clin Microbiol Rev* 27:463–481.
2. Tagaya Y, Gallo RC (2017) The exceptional oncogenicity of HTLV-1. *Front Microbiol* 8:1425.
3. Maman S, Witz IP (2018) A history of exploring cancer in context. *Nat Rev Cancer* 18: 359–376.
4. Buti L, et al. (2011) Helicobacter pylori cytotoxin-associated gene A (CagA) subverts the apoptosis-stimulating protein of p53 (ASPP2) tumor suppressor pathway of the host. *Proc Natl Acad Sci USA* 108:9238–9243.
5. Kaplan-Türköz B, et al. (2012) Structural insights into Helicobacter pylori oncoprotein CagA interaction with β1 integrin. *Proc Natl Acad Sci USA* 109:14640–14645.
6. Majumder M, Ghosh AK, Steele R, Ray R, Ray RB (2001) Hepatitis C virus NS5A physically associates with p53 and regulates p21/waf1 gene expression in a p53-dependent manner. *J Virol* 75:1401–1407.
7. Lan K-H, et al. (2002) HCV NS5A interacts with p53 and inhibits p53-mediated apoptosis. *Oncogene* 21:4801–4811.
8. Lamb A, Chen LF (2013) Role of the Helicobacter pylori-induced inflammatory response in the development of gastric cancer. *J Cell Biochem* 114:491–497.
9. Gallo RC (1999) Tat as one key to HIV-induced immune pathogenesis and Tat (correction of Pat) toxoid as an important component of a vaccine. *Proc Natl Acad Sci USA* 96:8324–8326.
10. Lin MV, King LY, Chung RT (2015) Hepatitis C virus-associated cancer. *Annu Rev Pathol* 10:345–370.
11. Human Microbiome Project Consortium (2012) Structure, function and diversity of the healthy human microbiome. *Nature* 486:207–214.
12. Yu T, et al. (2017) Fusobacterium nucleatum promotes chemoresistance to colorectal cancer by modulating autophagy. *Cell* 170:548–563.e16.

13. Bullman S, et al. (2017) Analysis of *Fusobacterium* persistence and antibiotic response in colorectal cancer. *Science* 358:1443–1448.
14. Yang Y, et al. (2017) Fusobacterium nucleatum increases proliferation of colorectal cancer cells and tumor development in mice by activating toll-like receptor 4 signaling to nuclear factor-κB, and up-regulating expression of MicroRNA-21. *Gastroenterology* 152:851–866.e24.
15. Purcell RV, Visnovska M, Biggs PJ, Schmeier S, Frizelle FA (2017) Distinct gut microbiome patterns associate with consensus molecular subtypes of colorectal cancer. *Sci Rep* 7:11590.
16. Yavlovich A, Katzenell A, Tarshis M, Higazi AAR, Rottem S (2004) Mycoplasma fermentans binds to and invades HeLa cells: Involvement of plasminogen and urokinase. *Infect Immun* 72:5004–5011.
17. Ainsworth JGE, Easterbrook PJ, Clarke J, Gilroy CB, Taylor-Robinson D (2001) An association of disseminated Mycoplasma fermentans in HIV-1 positive patients with non-Hodgkin's lymphoma. *Int J STD AIDS* 12:499–504.
18. Barykova YA, et al. (2011) Association of Mycoplasma hominis infection with prostate cancer. *Oncotarget* 2:289–297.
19. Henrich B, et al. (2014) Mycoplasma salivarium as a dominant coloniser of Fanconi anaemia associated oral carcinoma. *PLoS One* 9:e92297.
20. Cao S, et al. (2017) Potential malignant transformation in the gastric mucosa of immunodeficient mice with persistent Mycoplasma penetrans infection. *PLoS One* 12: e0180514.
21. Jiang S, Zhang S, Langenfeld J, Lo S-C, Rogers MB (2008) Mycoplasma infection transforms normal lung cells and induces bone morphogenetic protein 2 expression by post-transcriptional mechanisms. *J Cell Biochem* 104:580–594.

MICROBIOLOGY

22. Namiki K, et al. (2009) Persistent exposure to Mycoplasma induces malignant transformation of human prostate cells. *PLoS One* 4:e6872.

23. Zhang S, Tsai S, Lo S-C (2006) Alteration of gene expression profiles during mycoplasma-induced malignant cell transformation. *BMC Cancer* 6:116.

24. Logunov DY, et al. (2008) Mycoplasma infection suppresses p53, activates NF-kappaB and cooperates with oncogenic Ras in rodent fibroblast transformation. *Oncogene* 27:4521–4531.

25. Lo SC, et al. (1991) Newly discovered mycoplasma isolated from patients infected with HIV. *Lancet* 338:1415–1418.

26. Bosma GC, Custer RP, Bosma MJ (1983) A severe combined immunodeficiency mutation in the mouse. *Nature* 301:527–530.

27. Kirchgessner CU, et al. (1995) DNA-dependent kinase (p350) as a candidate gene for the murine SCID defect. *Science* 267:1178–1183.

28. Gurley KE, Vo K, Kemp CJ (1998) DNA double-strand breaks, p53, and apoptosis during lymphomagenesis in scid/scid mice. *Cancer Res* 58:3111–3115.

29. Nacht M, et al. (1996) Mutations in the p53 and SCID genes cooperate in tumorigenesis. *Genes Dev* 10:2055–2066.

30. Shultz LD, et al. (1995) Multiple defects in innate and adaptive immunologic function in NOD/LtSz-scid mice. *J Immunol* 154:180–191.

31. Jäättelä M (1995) Over-expression of hsp70 confers tumorigenicity to mouse fibrosarcoma cells. *Int J Cancer* 60:689–693.

32. Seo J-S, et al. (1996) T cell lymphoma in transgenic mice expressing the human Hsp70 gene. *Biochem Biophys Res Commun* 218:582–587.

33. Kaur J, Kaur J, Ralhan R (2000) Induction of apoptosis by abrogation of HSP70 expression in human oral cancer cells. *Int J Cancer* 85:1–5.

34. Calloni G, et al. (2012) DnaK functions as a central hub in the E. coli chaperone network. *Cell Rep* 1:251–264.

35. Clarke CF, et al. (1988) Purification of complexes of nuclear oncogene p53 with rat and Escherichia coli heat shock proteins: In vitro dissociation of hsc70 and dnaK from murine p53 by ATP. *Mol Cell Biol* 8:1206–1215.

36. Nihei T, Takahashi S, Sagae S, Sato N, Kikuchi K (1993) Protein interaction of retinoblastoma gene product pRb110 with M(r) 73,000 heat shock cognate protein. *Cancer Res* 53:1702–1705.

37. Pinhasi-Kimhi O, Michalovitz D, Ben-Zeev A, Oren M (1986) Specific interaction between the p53 cellular tumour antigen and major heat shock proteins. *Nature* 320:182–184.

38. Stürzbecher HW, Chumakov P, Welch WJ, Jenkins JR (1987) Mutant p53 proteins bind hsp 72/73 cellular heat shock-related proteins in SV40-transformed monkey cells. *Oncogene* 1:201–211.

39. Hupp TR, Meek DW, Midgley CA, Lane DP (1992) Regulation of the specific DNA binding function of p53. *Cell* 71:875–886.

40. Vassilev LT, et al. (2004) In vivo activation of the p53 pathway by small-molecule antagonists of MDM2. *Science* 303:844–848.

41. Xiong Y, et al. (1993) p21 is a universal inhibitor of cyclin kinases. *Nature* 366:701–704.

42. Yuan J, Luo K, Zhang L, Cheville JC, Lou Z (2010) USP10 regulates p53 localization and stability by deubiquitinating p53. *Cell* 140:384–396.

43. Godon C, et al. (2008) PARP inhibition versus PARP-1 silencing: Different outcomes in terms of single-strand break repair and radiation susceptibility. *Nucleic Acids Res* 36:4454–4464.

44. Schultz N, Lopez E, Saleh-Gohari N, Helleday T (2003) Poly(ADP-ribose) polymerase (PARP-1) has a controlling role in homologous recombination. *Nucleic Acids Res* 31:4959–4964.

45. Langelier M-F, Planck JL, Roy S, Pascal JM (2012) Structural basis for DNA damage-dependent poly(ADP-ribosyl)ation by human PARP-1. *Science* 336:728–732.

46. Amé JC, Spenlehauer C, de Murcia G (2004) The PARP superfamily. *BioEssays* 26:882–893.

47. Schreiber V, Dantzer F, Ame JC, de Murcia G (2006) Poly(ADP-ribose): Novel functions for an old molecule. *Nat Rev Mol Cell Biol* 7:517–528.

48. Pines A, et al. (2012) PARP1 promotes nucleotide excision repair through DDB2 stabilization and recruitment of ALC1. *J Cell Biol* 199:235–249.

49. Robu M, et al. (2013) Role of poly(ADP-ribose) polymerase-1 in the removal of UV-induced DNA lesions by nucleotide excision repair. *Proc Natl Acad Sci USA* 110:1658–1663.

50. Ruscetti T, et al. (1998) Stimulation of the DNA-dependent protein kinase by poly(ADP-ribose) polymerase. *J Biol Chem* 273:14461–14467.

51. Ying S, et al. (2016) DNA-PKcs and PARP1 bind to unresected stalled DNA replication forks where they recruit XRCC1 to mediate repair. *Cancer Res* 76:1078–1088.

52. Berwick M, Vineis P (2000) Markers of DNA repair and susceptibility to cancer in humans: An epidemiologic review. *J Natl Cancer Inst* 92:874–897.

53. de Murcia JM, et al. (1997) Requirement of poly(ADP-ribose) polymerase in recovery from DNA damage in mice and in cells. *Proc Natl Acad Sci USA* 94:7303–7307.

54. Wang ZQ, et al. (1997) PARP is important for genomic stability but dispensable in apoptosis. *Genes Dev* 11:2347–2358.

55. d'Adda di Fagagna F, et al. (1999) Functions of poly(ADP-ribose) polymerase in controlling telomere length and chromosomal stability. *Nat Genet* 23:76–80.

56. Morrison C, et al. (1997) Genetic interaction between PARP and DNA-PK in V(D)J recombination and tumorigenesis. *Nat Genet* 17:479–482.

57. Nunes JM, Mayer-Hartl M, Hartl FU, Müller DJ (2015) Action of the Hsp70 chaperone system observed with single proteins. *Nat Commun* 6:6307.

58. Clerico EM, Tilitsky JM, Meng W, Gierasch LM (2015) How hsp70 molecular machines interact with their substrates to mediate diverse physiological functions. *J Mol Biol* 427:1575–1588.

59. Costa TRD, et al. (2015) Secretion systems in Gram-negative bacteria: Structural and mechanistic insights. *Nat Rev Microbiol* 13:343–359.

60. Holland IB (2004) Translocation of bacterial proteins—An overview. *Biochim Biophys Acta Mol Cell Res* 1694:5–16.

61. Carrió MM, Villaverde A (2005) Localization of chaperones DnaK and GroEL in bacterial inclusion bodies. *J Bacteriol* 187:3599–3601.

62. Vega VL, et al. (2008) Hsp70 translocates into the plasma membrane after stress and is released into the extracellular environment in a membrane-associated form that activates macrophages. *J Immunol* 180:4299–4307.

63. Mambula SS, Stevenson MA, Ogawa K, Calderwood SK (2007) Mechanisms for Hsp70 secretion: Crossing membranes without a leader. *Methods* 43:168–175.

64. Thériault JR, Adachi H, Calderwood SK (2006) Role of scavenger receptors in the binding and internalization of heat shock protein 70. *J Immunol* 177:8604–8611.

65. Bendtsen JD, Kiemer L, Fausbøll A, Brunak S (2005) Non-classical protein secretion in bacteria. *BMC Microbiol* 5:58.

66. Warren JR, Marshall B (1983) Unidentified curved bacilli on gastric epithelium in active chronic gastritis. *Lancet* 1:1273–1275.

67. Arnheim Dahlström L, et al. (2011) Prospective seroepidemiologic study of human papillomavirus and other risk factors in cervical cancer. *Cancer Epidemiol Biomarkers Prev* 20:2541–2550.

68. Smith JS, et al.; IARC multicentric case-control study (2004) Chlamydia trachomatis and invasive cervical cancer: A pooled analysis of the IARC multicentric case-control study. *Int J Cancer* 111:431–439.

69. Stone KM, et al. (1995) Sexual behavior, sexually transmitted diseases, and risk of cervical cancer. *Epidemiology* 6:409–414.

70. Kumar S, Stecher G, Tamura K (2016) MEGA7: Molecular evolutionary genetics analysis version 7.0 for bigger datasets. *Mol Biol Evol* 33:1870–1874.

71. Tomasetti C, Li L, Vogelstein B (2017) Stem cell divisions, somatic mutations, cancer etiology, and cancer prevention. *Science* 355:1330–1334.

72. Romerio F, Zella D (2002) MEK and ERK inhibitors enhance the anti-proliferative effect of interferon-alpha2b. *FASEB J* 16:1680–1682.

73. Li M, et al. (2002) Deubiquitination of p53 by HAUSP is an important pathway for p53 stabilization. *Nature* 416:648–653.